

Dynamical exponent of a quantum critical itinerant ferromagnet: A Monte Carlo studyYuzhi Liu^{1,2}, Weilun Jiang^{1,2}, Avraham Klein³, Yuxuan Wang⁴, Kai Sun⁵, Andrey V. Chubukov⁶,
and Zi Yang Meng^{7,1,*}¹*Beijing National Laboratory for Condensed Matter Physics and Institute of Physics, Chinese Academy of Sciences, Beijing 100190, China*²*School of Physical Sciences, University of Chinese Academy of Sciences, Beijing 100190, China*³*Department of Physics, Faculty of Natural Sciences, Ariel University, Ariel*⁴*Department of Physics, University of Florida, Gainesville, Florida 32601, USA*⁵*Department of Physics, University of Michigan, Ann Arbor, Michigan 48109, USA*⁶*School of Physics and Astronomy, University of Minnesota, Minneapolis, Minnesota 55455, USA*⁷*Department of Physics and HKU-UCAS Joint Institute of Theoretical and Computational Physics, The University of Hong Kong, Pokfulam Road, Hong Kong SAR, China*

(Received 24 June 2021; accepted 12 January 2022; published 24 January 2022)

We consider the effect of the coupling between two-dimensional (2D) quantum rotors near an XY ferromagnetic quantum critical point and spins of itinerant fermions. We analyze how this coupling affects the dynamics of rotors and the self-energy of fermions. A common belief is that near a $q = 0$ ferromagnetic transition, fermions induce an Ω/q Landau damping of rotors (i.e., the dynamical critical exponent is $z = 3$) and Landau overdamped rotors give rise to non-Fermi liquid fermionic self-energy $\Sigma \propto \omega^{2/3}$. This behavior has been confirmed in previous quantum Monte Carlo (QMC) studies. Here we show that for the XY case the behavior is different. We report the results of large-scale quantum Monte Carlo simulations, which show that at small frequencies $z = 2$ and $\Sigma \propto \omega^{1/2}$. We argue that the new behavior is associated with the fact that a fermionic spin is by itself not a conserved quantity due to spin-spin coupling to rotors, and a combination of self-energy and vertex corrections replaces $1/q$ in the Landau damping by a constant. We discuss the implication of these results to experiments.

DOI: [10.1103/PhysRevB.105.L041111](https://doi.org/10.1103/PhysRevB.105.L041111)**I. INTRODUCTION**

In the study of strongly correlated systems, quantum criticality in itinerant fermionic systems is of crucial importance because it offers a pathway towards non-Fermi liquids and unconventional superconductivity (see for example Refs. [1–3] and references therein). In this study, we focus on ferromagnetic quantum critical points in itinerant fermion systems, where non-Fermi liquid (nFL) behaviors have been observed in the quantum critical region in a variety of materials, such as the Kondo lattice materials UGe_2 [4], URhGe [5], UCoGe [6], YbNi_4P_2 [7] and more recently CeRh_6Ge_4 [8,9], where in the latter a pressure-induced quantum critical point (QCP) with the characteristic power-law nFL specific heat and resistivity is reported. This experimental progress poses a series of theoretical questions on the origin and characterization of these nFL behaviors. In particular, it is of crucial importance to understand the fundamental principles that govern these QCPs and to identify the universal properties that are enforced by these principles.

On the theoretical side, extensive efforts have been devoted to this topic in the past few decades. Based on the Hertz-Millis-Moriya theory [10–12], the dynamic critical exponent of an itinerant ferromagnetic QCP, or indeed any

isotropic long-wavelength collective excitation with ordering vector $\mathbf{q} = 0$, is $z = 3$. The extension of the theory to study fermionic properties [13–17], predicts that fermions near such QCPs are overdamped, with fermionic self-energy scaling as $\Sigma \propto \omega_n^{2/3}$, where ω_n represents the Matsubara frequency. The fact that this power is less than 1 implies that the system is an nFL at low enough frequencies. Within the one-loop framework, these conclusions and scaling exponents are universal for all itinerant ferromagnetic QCPs. When higher-order contributions are taken into account, additional phenomena may appear, e.g., first-order behavior, spiral phases, and low-frequency scaling violations [17–25], as well as superconductivity. In particular, if the order parameter (OP) is nonconserved, higher-order processes modify the damping of the bosons in the long-wavelength limit, and usually change the value of z to 2 [26,27].

With the recent development in quantum Monte Carlo (QMC) techniques [28–32], it has become possible to simulate such fermionic systems at large scale in the close vicinity of the quantum critical point [33–35]. Such simulations offer an unbiased and accurate numerical measurement to examine and to test these theoretical ideas. In recent QMC studies on the itinerant (2 + 1)d ferromagnetic Ising quantum critical point, numerical results confirm the universal scaling relation predicted by the $z = 3$ theory [31,36]. The fermionic self-energy, properly extrapolated to $T = 0$ [36,37], agrees with the expected non-Fermi liquid $\omega^{2/3}$ behavior at low energies.

*zymeng@hku.hk

In this Letter, we study a ferromagnetic QCP in which the spin OP is of XY type. The key difference between an Ising-type and XY ferromagnetic QCP is that in the latter case a spin of an itinerant fermion is not separately a conserved quantity in the presence of a spin-spin interaction with a rotor, and the same is true for a rotor.

From large-scale QMC simulations, we show that instead of $z = 3$ and $\Sigma \propto \omega_n^{2/3}$, the scaling exponent becomes $z = 2$, and fermion self-energy becomes $\Sigma \propto \omega_n^{1/2}$. The mechanism driving this change is the form of the boson damping $\propto |\Omega_n|/\Gamma(q, \Omega_n)$. We find that $\Gamma(q, \Omega_n)$ for conserved and nonconserved OPs is very different, as Γ is constrained by a Ward identity in the conserved case only [26,27,38,39]. In our case we find $\Gamma(q, \Omega_n) \approx \Gamma_0$ is constant over a wide range of temperatures, frequencies and momenta, similar to that in an antiferromagnet. Such damping arises from scattering processes beyond the one-loop order and is generally associated with noncancellation between self-energy and vertex corrections (including Aslamazov-Larkin-type terms) [27]. Once this is introduced into the Hertz-Millis-Moriya framework, the bosonic dynamical exponent becomes $z = 2$, and the fermion self-energy gets modified to $\Sigma \propto \omega_n^{1/2}$.

II. MODEL AND PHASE DIAGRAM

We simulate lattice system composed of two identical fermion layers and one rotor layer as shown in Fig. 1(a), and the Hamiltonian is $\hat{H} = \hat{H}_f + \hat{H}_{qr} + \hat{H}_{\text{int}}$. The fermion part of the Hamiltonian is $\hat{H}_f = -t_1 \sum_{\langle(i,j)\rangle, \sigma, \lambda} \hat{c}_{i\sigma\lambda}^\dagger \hat{c}_{j\sigma\lambda} - t_2 \sum_{\langle\langle(i,j)\rangle\rangle, \sigma, \lambda} \hat{c}_{i\sigma\lambda}^\dagger \hat{c}_{j\sigma\lambda} + \text{H.c.}$, where $t_1 = 1$, $t_2 = 0.2$, $\langle \rangle$ ($\langle\langle \rangle\rangle$) denote (next) nearest neighbor, $\sigma = \uparrow$ or \downarrow is the spin index, and $\lambda = 1$ or 2 labels the two fermion layers. For the rotor layer, we define a quantum rotor model (QRM) on the same square lattice with a Hamiltonian $\hat{H}_{qr} = \frac{U}{2} \sum_i \hat{L}_i^2 - t_b \sum_{\langle(i,j)\rangle} \cos(\hat{\theta}_i - \hat{\theta}_j)$, where \hat{L}_i and $\hat{\theta}_i$ are the angular momentum and polar angle of the rotor at site i , respectively. In the simulations, we set $t_b = 1$ and use the ratio of U/t_b to tune the system through the QCP. Without fermions, the phase diagram of the rotor model is well known [32]. It contains two phases: paramagnetic and ferromagnetic. At finite temperatures, the ferromagnetic phase shows quasi-long-range order and the thermal phase transition is Berezinskii-Kosterlitz-Thouless (BKT) type. At $T = 0$, the ferromagnetic order becomes long range and the quantum phase transition belongs to the $(2 + 1)\text{d}$ XY universality class, which occurs at a QCP at $(U/t_b)_c = 4.25(2)$ [32]. The last term of the Hamiltonian \hat{H}_{int} couples a fermion spin ferromagnetically to a quantum rotor at the same site:

$$\hat{H}_{\text{int}} = -\frac{K}{2} \sum_i \hat{c}_i^\dagger \sigma \hat{c}_i \cdot \hat{\theta}_i, \quad (1)$$

where σ represents fermion spin, and $\hat{\theta}_i = (\cos \theta_i, \sin \theta_i)$. As we noted above, this coupling term breaks the spin symmetry for, separately, the fermions and the rotors, replacing it with a rotation symmetry of the total spin (rotors + fermions). We set the coupling strength to $K = 1$. We denote this model the XY-spin-fermion model.

In a recent study [35], we used a similar model with $K = 4$ to study the superconducting properties of this model,

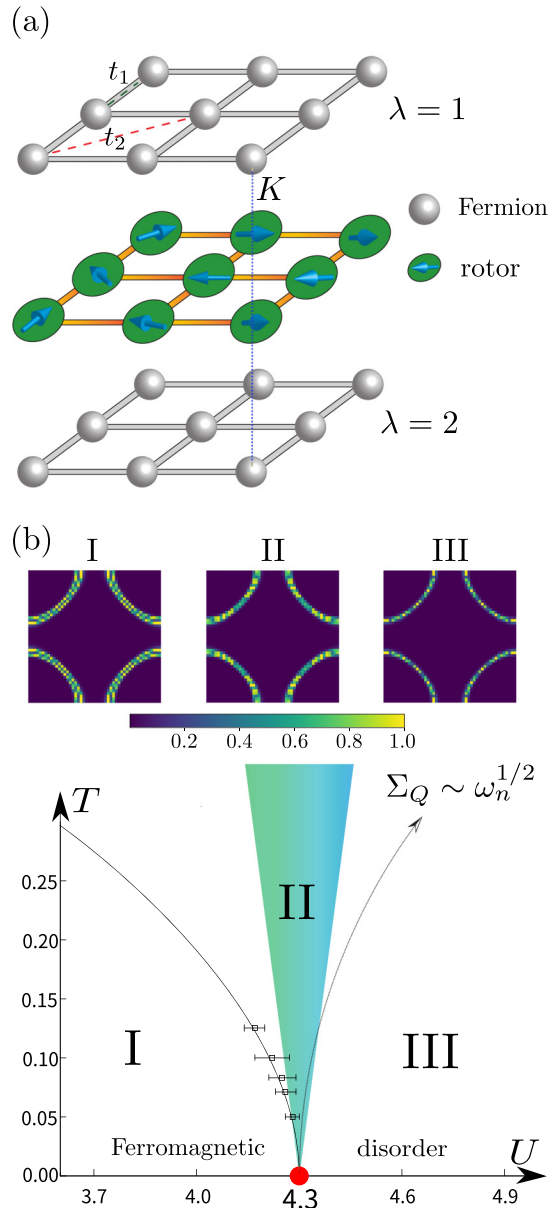


FIG. 1. Model and phase diagram. (a) The lattice model. The two identical layers of fermions ($\lambda = 1, 2$) with nearest-neighbor and next-nearest-neighbor hoppings $t_1 = 1$ and $t_2 = 0.2$ couple to the quantum rotor model in the middle layer with on-site coupling $K = 1$. As one tunes the rotors towards QCP, the entire system develops nFL behavior. (b) $T - U$ phase diagram. The QCP is located at $U_c = 4.30(3)$, and when $U < U_c$ the system acquires ferromagnetic (quasi) long-range order below the T_{BKT} boundary, which extrapolates to U_c , as denoted by the black solid line, with the finite temperature transition points determined in SM [40]. Panels near the top part of (b) show the Fermi surfaces, obtained from the dynamical Green's function $G(\mathbf{k}, \tau = \beta/2)$ of 12×12 size lattice with $\beta = 1/T = 24$, which correspond to the I($U = 4.0$), II($U = 4.3$), and III($U = 4.5$) regions of the phase diagram. In the ferromagnetic phase, the Fermi surface splits. In the vicinity of the QCP, an nFL phase emerges due to strong quantum critical fluctuations, and the Fermi surface smears out. In the disordered region, the Fermi surface is close to that of the free system (see SM [40]).

and found a pseudogap region and a superconducting dome around the QCP. While interesting on their own, these phenomena preempts the nonsuperconducting quantum-critical behavior of the system. In this work, we suppress superconductivity by utilizing a smaller value of K , driving the superconducting phase to unreachably low temperatures. This allows us to closely study the normal-state critical properties in the vicinity of the QCP, and reveal a wealth of interesting features.

We plot the phase diagram of this model in Fig. 1(b). Similar to the QRM, the XY-spin-fermion system also exhibits two phases, paramagnetic and ferromagnetic, although the QCP now moves from $U_c = 4.25(2)$ of the QRM to $U_c = 4.30(3)$ here. More importantly, the presence of fermionic degrees of freedom has crucial impact on the quantum criticality, altering the dynamical exponent of the rotor propagator. In return, coupling to soft rotor tends to make the fermions incoherent, with non-Fermi liquid self-energy.

III. RESULTS AND ANALYSIS

To study the scaling behavior of critical fluctuation, we measure the dynamic susceptibility of quantum rotors, $\chi(\mathbf{q}, \Omega_n) = \frac{1}{L^2} \int d\tau \sum_{ij} e^{i\Omega_n\tau - i\mathbf{q}\cdot\mathbf{r}_{ij}} \langle \theta_i(\tau)\theta_j(0) \rangle$ at $U_c = 4.30(3)$ and low temperatures, where $\Omega_n = 2n\pi T$ is the bosonic Matsubara frequency. At small Ω_n and q , we find the momentum dependence of χ^{-1} to scale with q^2 (see Supplemental Material (SM) [40]) as expected. However, in the frequency dependence, we observe a completely different behavior from the prediction of Hertz-Millis-Moriya theory. For a system with a conserved OP, it is well known that the Landau damping takes a singular form of $\frac{\Omega_n}{\sqrt{|\mathbf{q}|^2 + \Omega_n^2}}$, and the $q = 0$ susceptibility exhibits a discontinuity at zero frequency, i.e., $\lim_{\Omega_n \rightarrow 0} [\chi^{-1}(\mathbf{q} = 0, \Omega_n) - \chi^{-1}(\mathbf{q} = 0, \Omega_n = 0)]$ is finite. This form is the base for $z = 3$ dynamical critical exponent in the Hertz-Millis-Moriya theory, which has been observed in QMC studies of the Ising QCP [31]. In contrast, our simulation exhibits no such singularity. Instead, as shown Fig. 2, which contains two representative QMC results for $\mathbf{q} = (0, 0)$ and $(4\pi/L, 0)$, $\chi^{-1}(\mathbf{q}, \Omega_n)$ are smooth function of Ω_n without any discontinuity. This absence of singularity and discontinuity is our key observation, in direct contrast to the Hertz-Millis-Moriya theory as well as numerical results in the Ising-spin-fermion model [31]. Detailed data analysis reveals that within numerical uncertainty, $\chi^{-1}(0, \Omega_n) - \chi^{-1}(0, 0)$ scales linearly with Ω_n at low frequency (the fit in Fig. 2), and thus the scaling behavior of the dynamic susceptibility indicates that $z = 2$, analogous to an itinerant QCP in which an order breaks the translational symmetry (e.g., antiferromagnetic QCPs) [37,41].

We argue that this discrepancy is due to the nonconservation of the OP in the XY-spin-fermion model. At one-loop level, the correction to a bosonic propagator comes from a polarization bubble of free fermions, and the result is the classic Landau damping $\propto \frac{\Omega_n}{\sqrt{v_F^2|\mathbf{q}|^2 + \Omega_n^2}}$. For free fermions, the Landau damping arises whether or not the OP is conserved. Thus, at weak enough coupling, a discontinuity exists even for a nonconserved OP, as seen in, e.g., simulations of nematic QCPs [42]. For a conserved OP, this form holds at all orders

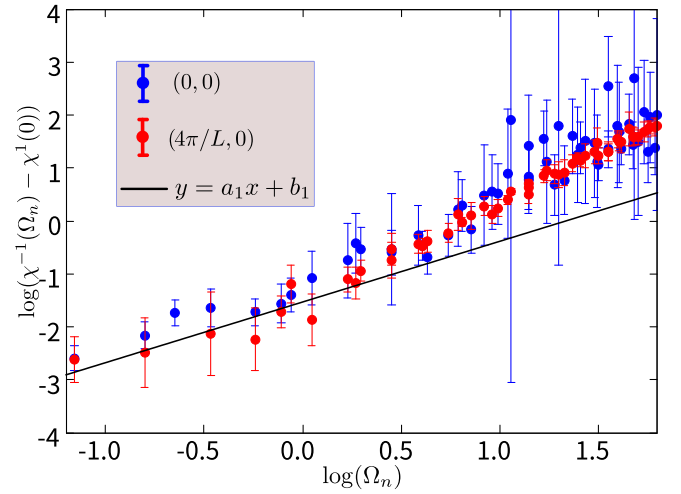


FIG. 2. Inverse bosonic susceptibility versus frequency at the QCP with $\mathbf{q} = (0, 0)$ and $(4\pi/L, 0)$. log-log plot for QMC data and fit the data in the range of $\log(\Omega_n) < 0$ by the black line. $a_1 = 1.14 \pm 0.2$, $b_1 = -1.53 \pm 0.1$ are fitting parameters and a_1 is very close to 1, which means the linear behavior at the small range $0 < \Omega_n < 1$.

in perturbation theory due to a Ward identity [23,27,43,44]. However, as we mentioned, in our XY-spin-fermion model, neither σ^x nor σ^y component of the fermion spin is conserved. In this situation, vertex and self-energy corrections to fermion polarization due to spin-spin coupling to rotors replace $1/\sqrt{v_F^2|\mathbf{q}|^2 + \Omega_n^2}$ by a constant Γ_0 , giving rise to damping $\propto \Omega_n/\Gamma_0 + \text{corrections}$ [26,27]. This changes the dynamical critical exponent to $z = 2$.

The change in z has an important consequence for the non-Fermi liquid fermion self-energy, which now must scale as $\omega^{1/2}$, in analogy to that for fermions at the hot spots of an antiferromagnetic QCP [16,41]. We verify this in our QMC data. Because simulations are performed at finite temperature with discrete Matsubara frequencies, a thermal contribution (corresponding to processes with zero internal bosonic Matsubara frequency) needs to be deducted from the fermion self-energy, in order to expose the nFL behavior. Procedures for this deduction of thermal background have been developed in Refs. [36,37], which we follow here (see SM [40] for details). In the temperature range of our QMC simulations the fermionic self energy remains small, and the fermions remain in a Fermi liquid state, so that the thermal contribution to fermion self-energy can be computed within Fermi liquid theory. It is

$$\Sigma(k_F, \omega_n) = \Sigma_T(\omega_n) + \Sigma_Q(\omega_n) = \frac{\alpha}{\omega_n} + \Sigma_Q(\omega_n), \quad (2)$$

where ω_n is the Matsubara frequency and Σ_T (Σ_Q) is the thermal (quantum) part of the self-energy. The thermal part scales as $\Sigma_T \propto 1/\omega_n$, while the quantum part is the $T = 0$ fermion self-energy,

$$\Sigma_Q = \bar{g}\sigma(\omega_n) \left(\frac{\omega_n}{\omega_c}\right)^{1/2} u \left(\frac{\omega_n}{\omega_c}\right) \quad (3)$$

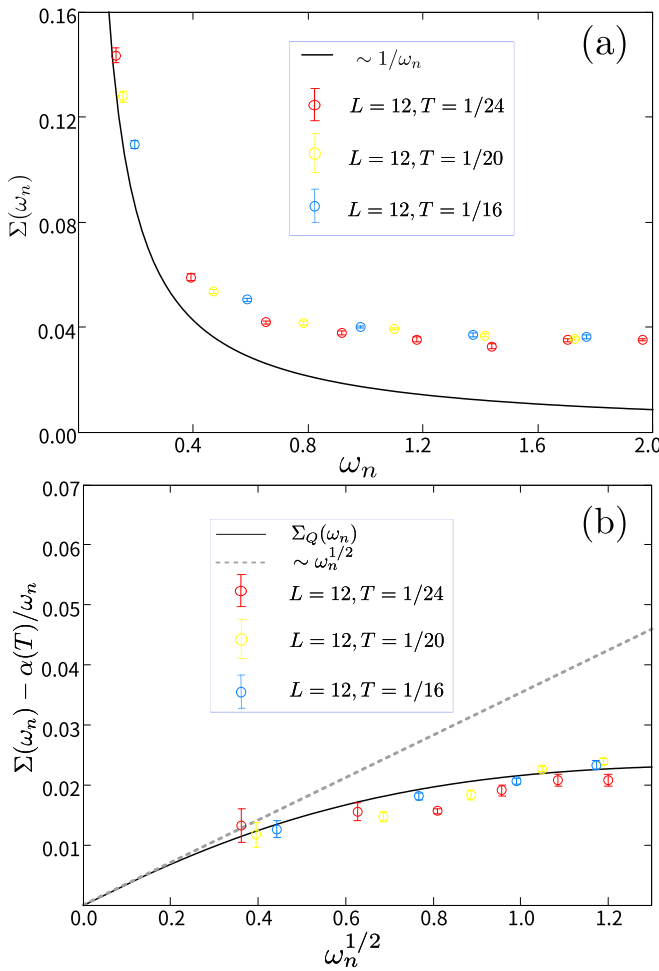


FIG. 3. Fermion self-energy. (a) $\Sigma(\mathbf{k}_F, \omega_n)$ from QMC at the QCP, here \mathbf{k}_F is along the (π, π) direction. The black line shows the thermal contribution, which scales as α/ω_n , $\alpha = 0.01705$. (b) The quantum part of fermionic self-energy at QCP (after subtracting thermal contributions). The black line shows theory prediction of the zero-temperature fermion self-energy [$\Sigma_Q(\omega_n)$], and the dashed line is its low-frequency asymptotic form of $\omega^{1/2}$.

with $\sigma(\omega_n)$ being the sign function and

$$u(z) = \int_0^\infty \frac{dx dy}{4\pi^2} \frac{1}{x^2 + y} \left(\frac{\sigma(y+1)}{\sqrt{1 + (\frac{y+1}{x})^2 z^2}} - \frac{\sigma(y-1)}{\sqrt{1 + (\frac{y-1}{x})^2 z^2}} \right), \quad (4)$$

where the $\omega_c = \kappa v_f^2$ and $u(z) \rightarrow \frac{1}{2\pi}$ when $z \rightarrow 0$. The value of the coefficient \bar{g} is given in the SM [40]. At small ω , the quantum part scales as $\Sigma_Q \propto \omega^{1/2}$.

We plot the fermion self-energy obtained from the QMC simulation at the QCP for the Fermi wave vector \mathbf{k}_F along the diagonal direction (Fig. 3). Because $\Sigma_T = \alpha/\omega_n$ and $\Sigma_Q \propto \sqrt{\omega_n}$, at low frequency, the self-energy is dominated by the thermal part. In Fig. 3(a), indeed the low-frequency data exhibits $1/\omega_n$ scaling (solid line), and the value of α can be obtained via numerical fitting. In Fig. 3(b), we subtract the thermal part, utilizing this numerical fitted α , and obtain Σ_Q . We also show the theoretical prediction for Σ_Q [Eq. (3)],

which agrees nicely with the QMC data. We emphasize that the data analysis only utilizes one fitting parameter (α), which is determined using only low-frequency data points, while good agreement is obtained for a large frequency window. As mentioned early on, the quantum part is the fermion self-energy at $T = 0$, and it scales as $\omega^{1/2}$ at low frequency, and this $\Sigma_Q \propto \omega^{1/2}$ asymptotic form is shown as the dashed line in Fig. 3(b).

IV. DISCUSSION

We showed numerically that the ferromagnetic fluctuations have critical scaling $z = 2$ and linear in frequency damping, giving rise to $\omega_n^{1/2}$ fermionic self-energy. The deviation from the expected $z = 3$ scaling and $\omega_n^{2/3}$ self-energy, is because Landau damping results from a delicate cancellation between scattering processes with different numbers of collective excitations, i.e., different loop order in a diagrammatic expansion [38,43,45]. Such cancellations occur only for a conserved OP, which in our system is the total spin, not separately the rotor spin or the fermion spin. As a result, the damping term in the rotor propagator is Ω_n/Γ_0 . For a purely fermionic system with a nonconserved OP (e.g., a nematic one), the dominant contribution to Γ_0 comes from thermally broadened fermions, in which case $\Gamma_0 \approx 2\Sigma_T$. Such behavior has been seen in previous QMC studies [35,37]. In the present case, a finite Γ_0 likely arises from the noncancellation between scattering processes involving different numbers of rotor propagators. We note that the model studied in Ref. [35] with $K = 4$ and the model studied here with $K = 1$ should in principle belong to the same universality class. However, the huge difference in energy scales between the models means we cannot conclusively connect the two phase diagrams, and we leave such an investigation to a further systematic study.

On the experimental side, whether the OP is conserved (Ising-like) or not (XY-like), depends on the structure (e.g., strength and sign) of the spin-orbit (SO) coupling. Thus, our results indicate that SO couplings play a crucial role here and dictate the scaling exponents of such QCPs, as well as the associated non-Fermi liquids. In materials with strong XY anisotropy, we expect, near a QCP, $z = 2$ and $\Sigma \propto \omega^{1/2}$.

The values of critical exponent have direct impact on the bosonic contribution to the specific heat. In two dimensions, for QCPs with conserved OPs, critical fluctuations generates a sublinear specific heat $C_V \propto T^{2/3}$ (with $z = 3$) [15], which dominates over the linear T contribution from the fermions. For nonconserved OPs, because $z = 2$, this specific heat scales as $C_V \propto T$ (up to logarithmic corrections), same as the fermion contribution. Thus, experimentally, these two universality classes can be distinguished. For three-dimensional (3D) systems, this specific heat anomaly is $C_V \propto T \ln(1/T)$ for QCPs with conserved OPs [11] and $C_V \propto T^{3/2}$ if the OP is nonconserved. Notice that $C_V \propto T^{3/2}$ is a subleading correction to the fermion contributions of $C_V \propto T$, and thus it can be easily distinguished from the $C_V \propto T \ln(1/T)$ anomaly of the conserved case. In addition to specific heat, critical fluctuations and non-Fermi-liquid behavior generate other experimental signatures, such as transport, spectroscopy, x-ray/neutron scatterings, magnetic resonance, etc. In QMC simulations, these physical observables can all be measured,

utilizing analytic continuations to convert imaginary time and Matsubara frequencies to real time and frequencies [35,46,47]. Such calculations will be performed in future studies, which can provide important guidance and insights for experimental studies in variety of quantum magnets, such as UGe_2 [4], URhGe [5], UCoGe [6], YbNi_4P_2 [7], and CeRh_6Ge_4 [8,9].

ACKNOWLEDGMENTS

We thank R. M. Fernandes, M. H. Christensen, Y. Schattner, X. Wang, and E. Berg for valuable discussions. Y.Z.L., W.L.J., and Z.Y.M. acknowledge support from the RGC of Hong Kong SAR of China (Grants No. 17303019, No. 17301420, and No. AoE/P-701/20) and the Strategic Priority Research Program of the Chinese Academy of Sci-

ences (Grant No. XDB33000000). We thank the Center for Quantum Simulation Sciences in the Institute of Physics, Chinese Academy of Sciences, the Computational Initiative at the Faculty of Science and the Information Technology Services at the University of Hong Kong and the Tianhe supercomputing platforms at the National Supercomputer Centers in Tianjin and Guangzhou for their technical support and generous allocation of CPU time. YW acknowledges support from NSF under Award No. DMR-2045871. The work by AVC was supported by the Office of Basic Energy Sciences, U.S. Department of Energy, under award DE-SC0014402. A.K. and A.V.C. acknowledge the hospitality of KITP at UCSB, where part of the work has been conducted. The research at KITP is supported by the National Science Foundation under Grant No. NSF PHY-1748958.

-
- [1] H. v. Löhneysen, A. Rosch, M. Vojta, and P. Wölfle, *Rev. Mod. Phys.* **79**, 1015 (2007).
- [2] S. Sachdev, *Quantum Phase Transitions*, 2nd ed. (Cambridge University Press, Cambridge, 2011).
- [3] S.-S. Lee, *Annu. Rev. Condens. Matter Phys.* **9**, 227 (2018).
- [4] A. D. Huxley, S. Raymond, and E. Ressouche, *Phys. Rev. Lett.* **91**, 207201 (2003).
- [5] F. Lévy, I. Sheikin, B. Grenier, and A. D. Huxley, *Science* **309**, 1343 (2005).
- [6] C. Stock, D. A. Sokolov, P. Bourges, P. H. Tobash, K. Gofryk, F. Ronning, E. D. Bauer, K. C. Rule, and A. D. Huxley, *Phys. Rev. Lett.* **107**, 187202 (2011).
- [7] A. Steppke, R. KÜchler, S. Lausberg, E. Lengyel, L. Steinke, R. Borth, T. Lühmann, C. Krellner, M. Nicklas, C. Geibel, F. Steglich, and M. Brando, *Science* **339**, 933 (2013).
- [8] B. Shen, Y. Zhang, Y. Komijani, M. Nicklas, R. Borth, A. Wang, Y. Chen, Z. Nie, R. Li, X. Lu, H. Lee, M. Smidman, F. Steglich, P. Coleman, and H. Yuan, *Nature (London)* **579**, 51 (2020).
- [9] Y. Wu, Y. Zhang, F. Du, B. Shen, H. Zheng, Y. Fang, M. Smidman, C. Cao, F. Steglich, H. Yuan, J. D. Denlinger, and Y. Liu, *Phys. Rev. Lett.* **126**, 216406 (2021).
- [10] J. A. Hertz, *Phys. Rev. B* **14**, 1165 (1976).
- [11] A. J. Millis, *Phys. Rev. B* **48**, 7183 (1993).
- [12] T. Moriya and Y. Takahashi, *Le Journal de Physique Colloques* **39**, C6-1466 (1978).
- [13] P. A. Lee, *Phys. Rev. Lett.* **63**, 680 (1989).
- [14] B. L. Altshuler, L. B. Ioffe, and A. J. Millis, *Phys. Rev. B* **50**, 14048 (1994).
- [15] V. Oganesyan, S. A. Kivelson, and E. Fradkin, *Phys. Rev. B* **64**, 195109 (2001).
- [16] A. Abanov, A. V. Chubukov, and J. Schmalian, *Adv. Phys.* **52**, 119 (2003).
- [17] J. Rech, C. Pépin, and A. V. Chubukov, *Phys. Rev. B* **74**, 195126 (2006).
- [18] T. R. Kirkpatrick and D. Belitz, *Phys. Rev. B* **67**, 024419 (2003).
- [19] D. Belitz, T. R. Kirkpatrick, and T. Vojta, *Rev. Mod. Phys.* **77**, 579 (2005).
- [20] D. L. Maslov and A. V. Chubukov, *Phys. Rev. B* **79**, 075112 (2009).
- [21] A. V. Chubukov, D. L. Maslov, and A. J. Millis, *Phys. Rev. B* **73**, 045128 (2006).
- [22] G. J. Conduit, A. G. Green, and B. D. Simons, *Phys. Rev. Lett.* **103**, 207201 (2009).
- [23] M. A. Metlitski and S. Sachdev, *Phys. Rev. B* **82**, 075127 (2010).
- [24] T. Holder and W. Metzner, *Phys. Rev. B* **92**, 041112(R) (2015).
- [25] A. G. Green, G. Conduit, and F. Krüger, *Annu. Rev. Condens. Matter Phys.* **9**, 59 (2018).
- [26] V. P. Mineev, *Phys. Rev. B* **88**, 224408 (2013).
- [27] A. V. Chubukov, J. J. Betouras, and D. V. Efremov, *Phys. Rev. Lett.* **112**, 037202 (2014).
- [28] H. Shi and S. Zhang, *Phys. Rev. E* **93**, 033303 (2016).
- [29] J. Liu, H. Shen, Y. Qi, Z. Y. Meng, and L. Fu, *Phys. Rev. B* **95**, 241104(R) (2017).
- [30] X. Y. Xu, Y. Qi, J. Liu, L. Fu, and Z. Y. Meng, *Phys. Rev. B* **96**, 041119(R) (2017).
- [31] X. Y. Xu, K. Sun, Y. Schattner, E. Berg, and Z. Y. Meng, *Phys. Rev. X* **7**, 031058 (2017).
- [32] W. Jiang, G. Pan, Y. Liu, and Z. Y. Meng, [arXiv:1912.08229](https://arxiv.org/abs/1912.08229).
- [33] E. Berg, S. Lederer, Y. Schattner, and S. Trebst, *Annu. Rev. Condens. Matter Phys.* **10**, 63 (2019).
- [34] X. Y. Xu, Z. H. Liu, G. Pan, Y. Qi, K. Sun, and Z. Y. Meng, *J. Phys.: Condens. Matter* **31**, 463001 (2019).
- [35] W. Jiang, Y. Liu, A. Klein, Y. Wang, K. Sun, A. V. Chubukov, and Z. Y. Meng, [arXiv:2105.03639](https://arxiv.org/abs/2105.03639).
- [36] X. Y. Xu, A. Klein, K. Sun, A. V. Chubukov, and Z. Y. Meng, *npj Quantum Mater.* **5**, 65 (2020).
- [37] A. Klein, A. V. Chubukov, Y. Schattner, and E. Berg, *Phys. Rev. X* **10**, 031053 (2020).
- [38] A. V. Chubukov and D. L. Maslov, *Phys. Rev. Lett.* **103**, 216401 (2009).
- [39] M. Punk, *Phys. Rev. B* **94**, 195113 (2016).
- [40] See Supplemental Material at <http://link.aps.org/supplemental/10.1103/PhysRevB.105.L041111> for QMC implementation of the model and the fitting of the QMC data are given, which includes Refs. [27,31,32,35–37,48,49].
- [41] Z. H. Liu, G. Pan, X. Y. Xu, K. Sun, and Z. Y. Meng, *Proc Natl Acad Sci USA* **116**, 16760 (2019).

- [42] Y. Schattner, S. Lederer, S. A. Kivelson, and E. Berg, *Phys. Rev. X* **6**, 031028 (2016).
- [43] A. V. Chubukov, *Phys. Rev. B* **72**, 085113 (2005).
- [44] A. Klein, S. Lederer, D. Chowdhury, E. Berg, and A. Chubukov, *Phys. Rev. B* **97**, 155115 (2018).
- [45] D. L. Maslov and A. V. Chubukov, *Rep. Prog. Phys.* **80**, 026503 (2016).
- [46] A. W. Sandvik, *Phys. Rev. E* **94**, 063308 (2016).
- [47] C. Zhou, Z. Yan, H.-Q. Wu, K. Sun, O. A. Starykh, and Z. Y. Meng, *Phys. Rev. Lett.* **126**, 227201 (2021).
- [48] R. Blankenbecler, D. J. Scalapino, and R. L. Sugar, *Phys. Rev. D* **24**, 2278 (1981).
- [49] F. F. Assaad, *Phys. Rev. B* **65**, 115104 (2002).